View Article Online
View Journal

Dalton Transactions

An international journal of inorganic chemistry

Accepted Manuscript

This article can be cited before page numbers have been issued, to do this please use: H. Gildenast, L. Gruszien, F. Friedt and U. Englert, *Dalton Trans.*, 2022, DOI: 10.1039/D2DT00728B.

ROYAL SOCIETY OF CHEMISTRY

rsc.li/dalton

View Article Online
DOI: 10.1039/D2DT00728B

Journal Name

ARTICLE TYPE

Cite this: DOI: 00.0000/xxxxxxxxxx

Phosphorus or Nitrogen - The first Phosphatriptycene in Coordination Polymer Chemistry.†

Hans Gildenast,[a] Lukas Gruszien,[a] Felix Friedt,[a] and Ulli Englert*[a,b]

Received Date
Accepted Date

DOI: 00.0000/xxxxxxxxxx

Phosphasilatriptycene, a phenylene spacer and a pyridyl moiety represent the building blocks of TRIP-Py, the first heteroditopic ligand featuring a phoshatriptycene scaffold. The P and N donor sites located at opposite ends of the prolate TRIP-Py molecule selectively coordinate metal cations matching their Pearson character. The harder pyridyl donor binds to Zn^{II}, the softer phosphorus donor to Pt^{II}, Hg^{II} and Au^{I}. The remarkably short Au−P bond in the latter underlines the good π acceptor character of the phoshatriptycene moiety. When both the chloride salts of hard Zn^{II} and soft Au^{I} cations are available for coordination, TRIP-Py acts as selective ditopic linker in the discrete trinuclear mixed-metal complex $[ZnCl_2(TRIP{-}PyAuCl)_2]$. For Cd^{II}, a cation with intermediate Pearson character, selectivity withers, and a monometallic coordination polymer is obtained. Its significantly elongated Cd−P coordinative bonds underline, however, the preference of Cd^{II} for the harder N donor. When Zn^{II} and Hg^{II} halides are combined, their preference for the matching donor sites in TRIP-Py and for tetrahedral coordination afford 1D and 2D heterobimetallic polymers with and without solvent-accessible voids. TRIP-Py enables the use of two important analytical tools: its rigidity facilitates crystallization and allowed to investigate 14 crystalline solids, and its P donor provides a powerful NMR probe for coordination.

1 Introduction

The chemistry of coordination polymers (CPs) and metal-organic frameworks (MOFs) is developing rapidly.[1–5] The plethora of potentially useful organic molecules and the special properties of metal cations allow new compounds and materials to both be refined for established applications like optics,[6,7] catalysis,[8–10] magnetism[11] and chemical separation[12–14] as well as to be designed for specialised applications such as cancer therapy,[15] proton transport for fuel cells,[16] electrochemical sensors[17] or magnetic refrigeration.[18] Leaving the classical crystalline CPs and MOFs, their amorphous and glassy relatives are also under investigation.[19]

Most of these materials contain a single type of metal cation and one or more polytopic ligands. Unequally less research is concerned with the selective incorporation of multiple different metal cations in the same compound, which is inherently synthetically more challenging.[20,21] Nevertheless, this greatly enhances the structural variety and, accordingly, enables a more precise customisation of a material and suggests new applications.[22]

Independent of mono- or heterometallic compounds, the ligand design for CPs and MOFs usually follows a few key principles: the ligand should feature two or more coordination sites which are spacially separated to avoid chelation. These coordination sites should feature strong donors to yield a stable compound. If a porous material is desired, the geometry between the coordination sites should be sufficiently rigid to support the pores upon desolvation.[23–25]

While the ligands designed for polymers with a single type of metal cation mostly exhibit multiple copies of the same coordination site, e.g. in 4,4'-bipyridine,[13,26] the selective coordination of two different metal cations is most often achieved by using heteropolytopic ligands with at least two distinctly different coordination sites with a discrepancy in their respective Pearson hardness.[27] A well ordered heterobimetallic polymer can then be achieved by a stepwise coordination of the two metal cations.[28–32]

Most examples combine one or more *hard* anionic oxygen donor atoms such as carboxylates and β-diketonates with a *softer* neutral nitrogen donor function to achieve a selective coordina-

[a] *RWTH Aachen University, Institute of Inorganic Chemistry, Landoltweg 1, 52074 Aachen, Germany. Fax: +49 241 8092288; Tel: +49 241 8094666; E-mail: ullrich.englert@ac.rwth-aachen.de*

[b] *Key Laboratory of Materials for Energy Conversion and Storage, Institute of Molecular Science, Shanxi University, Taiyuan, Shanxi 030006, People's Republic of China.*

† Electronic supplementary information (ESI) available: Refinement and Crystal Structure Details, PXRD patterns, NMR spectra, X-ray crystallographic tables and CCDC 2155645-2155658. See DOI: 00.0000/00000000.

View Article Online
DOI: 10.1039/D2DT00728B

tion.[33–36] Few others expand this scope to sulphur, carbon and phosphorus donors on the soft coordination site while retaining the anionic oxygen based donor.[37–40] The need for deprotonation additionally increases selectivity by introducing different reaction conditions for the two coordination sites, and this contribution can hardly be separated from the effect of the Pearson character. In order to address only the latter issue and possibly construct heterobimetallic CPs purely by selectivity through the Pearson character, we envisaged to use a heteroditopic ligand with two different neutral coordination sites, namely an N donor as the harder and a P donor as the softer coordination site. That this combination can display selectivity has been demonstrated numerous times in discrete bimetallic complexes.[41–44] There are even quite a few examples of P,N heteroditopic ligands that form coordination polymers, however, all of these were monometallic CPs.[45–64]

With our ligand design we want to adhere as closely as possible to the key principals mentioned above which is straightforward for the N donor by choosing a pyridine moiety. Inclusion of a phosphorus donor into a linear and semi-rigid scaffold poses a greater challenge. The equivalent phosphabenzene motive is inherently air sensitive[65] and the more stable triarylphosphines are flexible and tend to form discrete supramolecules.[40] Both issues can be rectified at the same time. Caged phosphines enable a fixed direction of the phosphorus lone pair with respect to the remaining ligand structure and at the same time they are predominantly air stable.[66] We chose the air stable 9-phosphatriptycene scaffold as a candidate to prepare a heteroditopic ligand and aimed to combine it with a pyridyl donor. While the coordination chemistry of pyridine derivatives has been exhaustively investigated, the number of coordination compounds with phosphatriptycene derivatives is almost negligible. Even if the secondary bridgehead atom is left unspecified, as there are a few atom types to chose from (Figure 1), there are only 18 entries to this date‡ in the CSD.[67]

In general, the geometric constraint of the phosphatriptycene enforces acute C−P−C angles and higher p character of the orbitals involved, lowering the basicity and σ-donor strength of the phosphorus lone pair.[68–72] At the same time, the π-acceptor strength increases which should favour the coordination of soft transition metal cations with high numbers of electrons in d orbitals.[73] Complexes have so far been documented for the metal cations Co^{II}, Fe^{II}, Pd^{II}, Pt^{II}, Rh^{I} and Au^{I}.[74,75] For a few Pd^{II} and Rh^{I} complexes catalysis has been tested and activity has been found to depend highly on the bridgehead atom.[76,77] For the latter we chose silicon. This affords an overall neutral ligand which should be inert to most reaction conditions required for coordination of either site. Both is also true for the carbon analogue, but the preparation of the silicon derivative is both more simple from a synthetic point of view and the procedure allows a modular adaption of the functional group attached to the triptycene scaffold.[78] One might also consider the aza derivative by Hellwinkel and Schenk[79] as a ditopic ligand, but triarylamines are rather unsuitable as ligands. Finally, we devised 10-(4-(4-pyridyl)-phenyl)-9-phospha-10-silatriptycene (TRIP-Py, **4**, Figure 1) for the investigation of P,N heterobimetallic CPs, a rigid, neutral molecule and the first heteroditopic phosphatriptycene.

‡January 5th, 2022

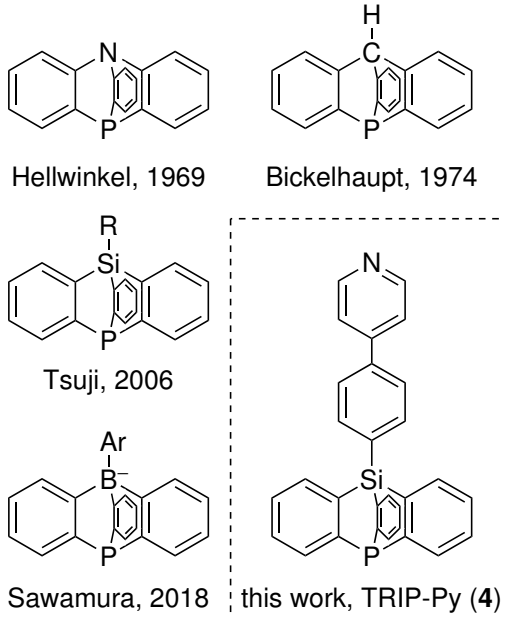

Fig. 1 Four types of 10-hetero-9-phosphatriptycenes from different authors and our ligand.

2 Results and Discussion

2.1 Ligand synthesis

The ligand 10-(4-(4-pyridyl)-phenyl)-9-phospha-10-silatriptycene (TRIP-Py, **4**) was prepared similar to the route established by Tsuji et al. (Figure 2),[78] with slight modifications for safety.

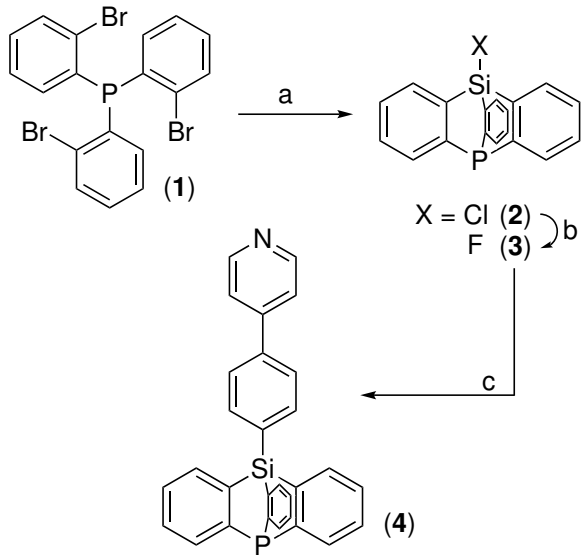

Fig. 2 Synthesis scheme for the ligand **4**. a: 1. 6 eq. *t*-BuLi in THF/Et_2O 2. $SiCl_4$ 3. TMSCl; b: $(NH_4)_2SiF_6$ in DME; c: 4-(4-bromophenyl)pyridine, *t*-BuLi.

View Article Online
DOI: 10.1039/D2DT00728B

The 9-phospha-10-silatriptycene scaffold is prepared by triple lithiation of tri-2-bromophenyl-phosphine (**1**) and reaction with $SiCl_4$. The subsequent halogen exchange to fluorine enables the following reaction with a carbon nucleophile. This does not work with the Si−Cl derivative which is evident as it does not react with the excess *t*-BuLi in the first step. The higher reactivity of the Si−F bond in the case of sterically encumbered silicon electrophiles is caused by the smaller radius of the fluorine as well as the stronger electrophilicity of the silicon induced by the high electronegativity of fluorine.[80] Tsuji and coworkers used HF in a large excess for this halogen exchange. To circumvent the challenging experimental requirements and potential safety hazards of HF we used $(NH_4)_2SiF_6$ in dimethoxyethane as a safer fluorine source. A similar reactivity was demonstrated by Damrauer and coworkers.[81] The final reaction step with the lithiated 4-phenylpyridine gives **4** in an acceptable yield of 29% over 3 steps. We also attempted the synthesis of the shorter version of this ligand without the phenylene spacer between the triptycene scaffold and the pyridyl ring. This would require the use of 4-bromopyridine as a starting material, an organic compound which in its pure form rapidly self polymerises giving a dark red cationic polymer. Several articles describe the isolation and lithiation of 4-bromopyridine without self polymerisation in diluted solution, but this approach was unsuccessful for our attempted synthesis. In contrast, 4-(4-bromophenyl)pyridine is a stable solid and the reaction with this pyridine source worked immediately.

Crystallization attempts afforded two polymorphs and a hemi-ethyl acetate solvate of **4**. The crystal structures and the polymorphism are discussed in the Supporting Information (section S1.1). While the triptycene scaffold is inherently very rigid, the overall ligand shows a minor degree of conformational flexibility which we will express with the help of two numerical parameters. The first quantity η measures linearity and simply corresponds to the angle P···Si···N. The second parameter ω represents the relative position of the phenylene ring to the triptycene scaffold as shown in Figure 3. With respect to the second quantity, a staggered conformation may be expected to minimise steric repulsion.
Figure 4 shows a scatter plot of all values for ω and η we collected so far from single crystal analyses. It reveals that ω can adopt virtually any value between the completely staggered and the eclipsed conformation. In contrast to our initial expectation the energy barrier between the staggered and eclipsed conformation appears to be very low. Based on a simple MM2[82] force field estimation as implemented in Chem3D[83] it is lower than 9 kJ mol^{-1}.

For reference, the rotational barrier about the C-C bond in ethane is estimated to be about 11 kJ mol^{-1} by MM2, in good agreement with the results from ab initio methods.[84] Independent of the correct estimation of the barrier it is evidently low enough to be overcome both in the solid by packing interactions as well as in solution. The latter results in a single set of signals for the triptycene protons in the ^{1}H-NMR spectrum (Supporting Information

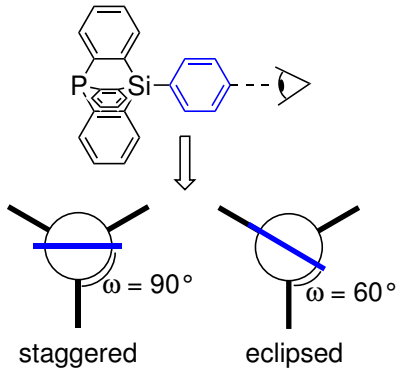

Fig. 3 Schematic representation of the conformational extremes for the angle ω which is defined as the largest of the angles between the mean plane of the phenylene ring of **4** between the triptycene and the pyridyl moiety and each of the triptycene rings. The pyridyl ring is omitted for clarity.

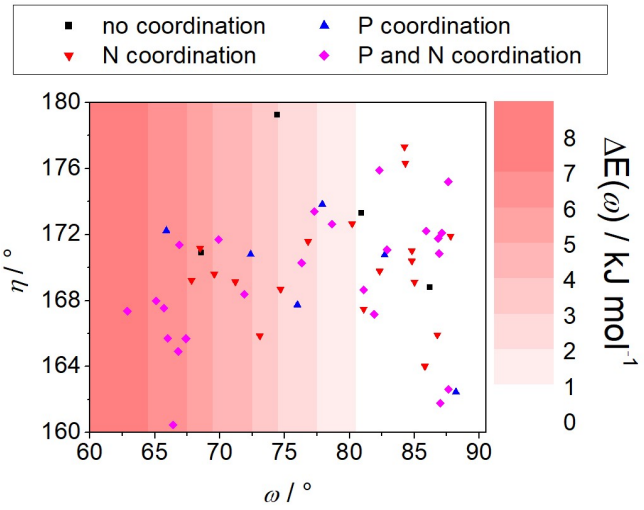

Fig. 4 Scatter plot of the parameters ω and η for the 14 crystal structures presented in this study and further TRIP-Py derivatives prepared by us but not reported in this article. The red background intensity encodes the energy obtained from a MM2[82] conformational analysis as implemented in Chem3D;[83] this energy scan corresponds to a pure ω rotation.

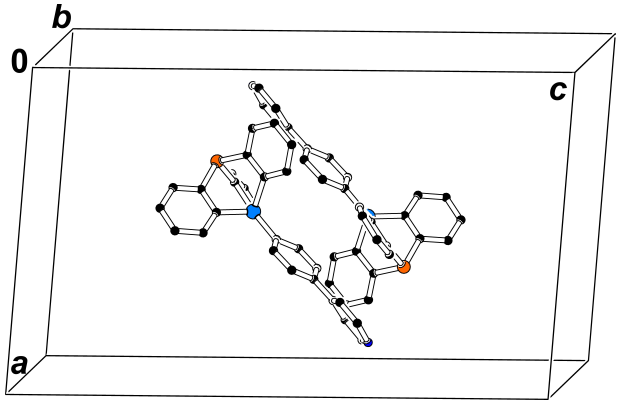

Fig. 5 Excerpt of the packing of **4**β showing two symmetry equivalent molecules by inversion. Each molecule embraces the pyridyl moiety of its neighbour with one of the triptycene grooves.

View Article Online
DOI: 10.1039/D2DT00728B

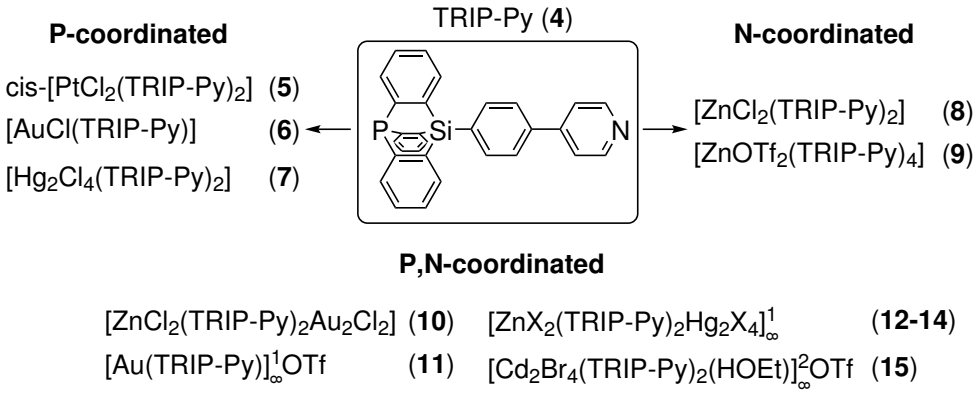

Fig. 6 Overview of the compounds presented in this article. The coordination compounds are sorted by the donor which is coordinated to the metal cation(s).

section 3.1). The η angle adopts values between 160° and 180° which is consequently not ideally linear but sufficiently close to 180° to consider TRIP-Py as a rod-shaped linker in terms of connectivity and crystal design. No strong correlation between the two geometry descriptors is observed. The tendency of the η values does, however, appear to scatter wider with an increase in ω.

The non-polar nature of **4** results in an absence of specific directional intermolecular contacts. The most prominent packing feature found in the crystal structures of the uncoordinated molecule and a series of its metal complexes is the embrace of two TRIP-Py entities with each other, with the pyridyl ring of one molecule situated inside one of the three triptycene grooves of its neighbour (Figure 5).

Before attempting the preparation of heterobimetallic coordination polymers it is advisable to test the selectivity of the different donor sites in isolation. An overview of the coordination compounds presented in this article is given in Figure 6.

2.2 P Coordination

Selective P coordination could be achieved with the soft 5d metal cations Pt^{II}, Au^{I} and Hg^{II}. The former two can be observed with NMR spectroscopy as the resulting chloride complexes *cis*-[$PtCl_2$(TRIP−Py)$_2$] (**5**) and [AuCl(TRIP−Py)] (**6**) are sufficiently soluble. Both display a prominent downfield shift and in the case of **5** the expected ^{195}Pt satellites (Supporting Information section 3.2) with a coupling constant of $J = 3782$ Hz corresponding to the *cis* isomer.[85] The selectivity is also reflected in the ^{1}H NMR because only the triptycene protons shift upon addition of the metal cations while the pyridyl protons remain stationary. The linear AuCl complex **6** and the insoluble [Hg_2Cl_4(TRIPPy)$_2$] (**7**) both give well behaved single crystals. **6** crystallises in the triclinic space group $P\bar{1}$ with $Z = 2$ (Figure 7).
With a length of 2.2184(11) Å the P−Au bond is remarkably short compared to other triarylphosphines (Figure 8) underlining the strong π-acidity of the phosphatriptycene moiety.[73]

Compound **7** crystallises in a dimeric structure in the triclinic space group $P\bar{1}$ with $Z = 1$ (Figure 9) and is to the best of our knowledge the first Hg complex of a phosphatriptycene. The two Hg^{II} cations are related by inversion ($\bar{1}$ on Wyckoff position 1*h*) and are bridged by two chlorido ligands. The fourfold coordination sphere is best described as trigonal pyramidal, with a τ_4 value of 0.79.[86] The three closest neighbours subtend a triangle about Hg1, and a significantly more distant symmetry equivalent of Cl1 (by inversion about Wyckoff Position 1*h*)

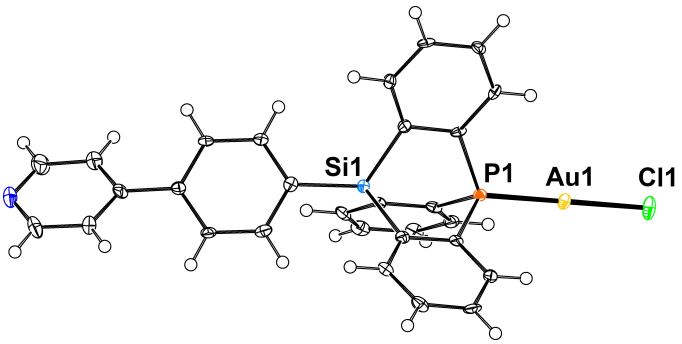

Fig. 7 Displacement ellipsoid plot of **6** (50% probability). Selected interatomic distances (Å) and angles (°): Au1−P1 2.2184(11), Au1−Cl1 2.2790(11), P1−Au1−Cl1 176.89(5), Si1···P1−Au1 177.86(6).

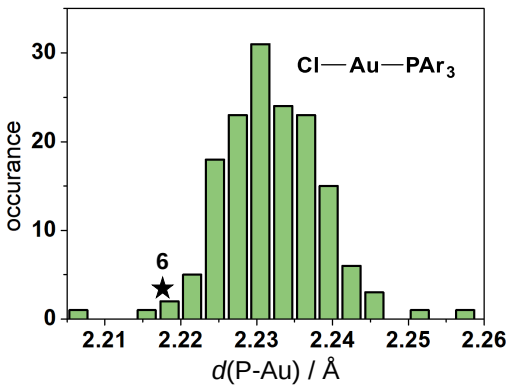

Fig. 8 Histogram of the P−Au distances in linear triarylphosphines complexes. The search was limited to error-free datasets collected at $T \leq 200$ K with $R_1 \leq 0.05$ and polymers and disordered structures were excluded.

View Article Online
DOI: 10.1039/D2DT00728B

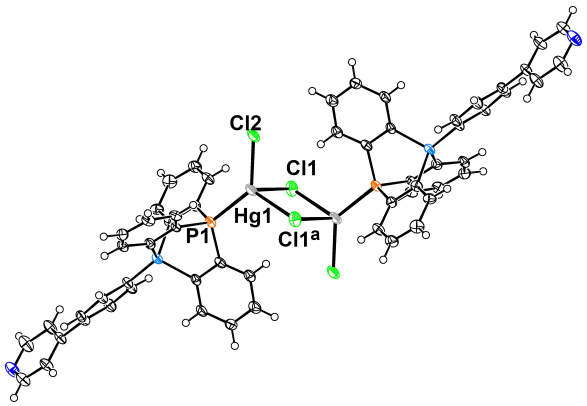

Fig. 9 Displacement ellipsoid plot of **7** (50% probability; solvent molecules omitted). Selected interatomic distances (Å): Hg1−P1 2.4022(19), Hg1−Cl1 2.535(2), Hg1−Cl1^a 2.7806(19), Hg1−Cl2 2.3900(18); $\tau_4(\text{Hg1}) = 0.79$, Var(X-Hg1-Y) = 274.28 °^{2}. Symmetry operation a: $1-x, 1-y, 1-z$.

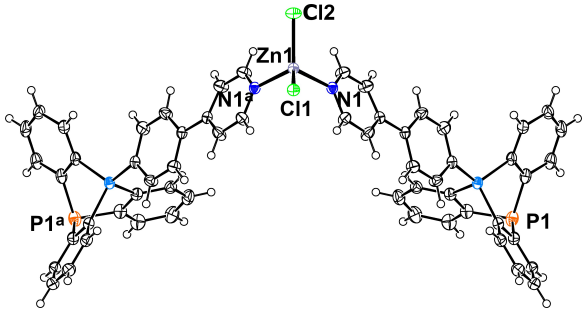

Fig. 10 Displacement ellipsoid plot of **8** (50% probability). Solvent molecules have been omitted for clarity. Selected interatomic distances (Å): Zn1−Cl1 2.1983(13), Zn1−Cl2 2.2380(13), Zn1−N1 2.056(2), N1−Zn1−N1^a 97.89(7), P1···Zn1···P1^a 77.12(2); $\tau_4(\text{Zn1}) = 0.91$, Var(X-Zn1-Y) = 61.2 °^{2}, Symmetry operation a: $x, 1.5-y, z$.

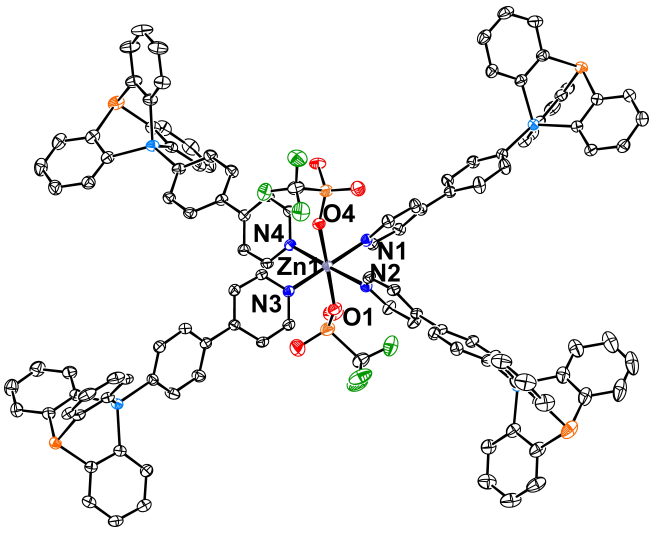

Fig. 11 Displacement ellipsoid plot of **9** (50% probability). Selected interatomic distances (Å): Zn1−O1 2.187(3), Zn1−O4 2.190(3), Zn1−N1 2.145(3), Zn1−N2 2.157(3), Zn1−N3 2.123(3), Zn1−N4 2.136(3), Var(X-Zn1-Y) = 5.62 °^{2}.

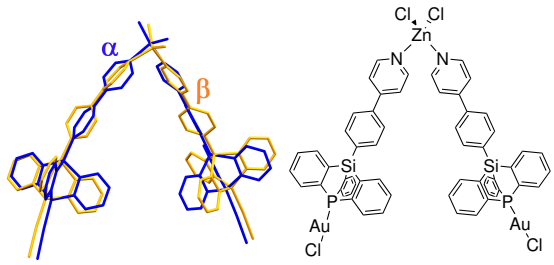

Fig. 12 Structure overlyay **10**α (blue) and **10**β (orange) generated with Mercury.[87]

occupies the apex of the pyramid. An additional weak contact exists between Hg1 and a THF molecule disordered about an inversion center (Wyckoff position 1*f*).

2.3 N Coordination

Selective N coordination can be achieved with Zn^{II} cations. The reaction with $ZnCl_2$ gives the tetrahedral complex [$ZnCl_2$(TRIP-Py)$_2$] (**8**) which crystallises in the orthorhombic space group *Pnma* with $Z = 4$ alongside partially occupied chloroform molecules (Figure 10). The structure features the Zn^{II} cation on the crystallographic mirror plane. It resides in regular tetrahedral coordination by a chlorido and an N-coordinated TRIP-Py ligand in general position and their symmetry equivalents. The ligand is not strictly linear, as evidenced by the fact that the angle P···Zn···P is smaller than N−Zn−N.

The ^{1}H NMR of a solution displays a clear shift of the protons in close proximity to the pyridyl moiety whereas the triptycene protons and the phosphorus signal remain stationary (Supporting Information section 1.6).

The same selectivity is observed for salts of weakly coordinating anions such as trifluoromethanesulfonate (OTf^-). The coordination to $Zn(OTf)_2$ gives the complex [$Zn(OTf)_2$(TRIP-Py)$_4$] (**9**) which crystallises in the triclinic space group $P\bar{1}$ with $Z = 2$ (Figure 11). The regular octahedral coordination sphere is formed by four of the pyridyl moieties in the equatorial plane and two axially coordinated OTf^- anions. The four pyridyl ligands form a propeller like structure to minimise inter-ligand steric repulsion. The structure features large solvent filled channels between the complexes which are filled with chlorobenzene and pentane molecules.

2.4 P,N bimetallic Coordination

The motives of the linear AuCl and the tetrahedral $ZnCl_2$ TRIP-Py complexes can be combined to yield a discrete heterobimetallic compound [$ZnCl_2$(TRIP-Py)$_2$Au$_2$Cl$_2$] (**10**). It can crystallise as two different chloroform solvates **10**α and **10**β which despite their completely different packing are remarkably similar with respect to the conformation of the heterometallic target complex (Figure 12). The crystal structure details and solution analytics are discussed in the Supporting Information (section 1.6).

Selectivity of the soft phosphine towards the terminal Au^I is compromised once the second coordination site becomes available.

View Article Online
DOI: 10.1039/D2DT00728B

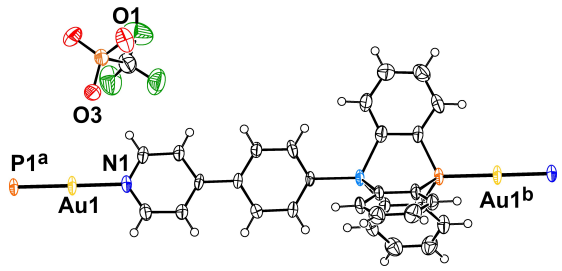

Fig. 13 Displacement ellipsoid plot of **11** (50% probability). The cocrystallised solvent molecule has been omitted for clarity. Selected interatomic distances (Å) and angles (°): Au1–P1^a 2.233(2), Au1–N1 2.081(6), Au1···O1c 3.269(6), P1^a–Au1–N1 176.35(17); Symmetry operations a: $1-x, 1-y, 1-z$.

The presence of a stoichiometric amount of OTf^- anions in a solution of **6** suffices to precipitate the linear cationic polymer $[Au(TRIP\text{-}Py)]^1_\infty OTf{\cdot}CHCl_3$ (**11**) even when more equivalents of ligand are added. The compound crystallises in the triclinic space group $P\bar{1}$ with $Z = 2$. The Au^I cation is coordinated by both the phosphatriptycene moiety as well as by the pyridyl, and the resulting 1D polymer propagates in [1 1 1] direction (Figure 13).

The OTf^- anion is located in close proximity between two symmetry equivalent Au^I cations. The shortest distance is 3.268 Å to one of the anion oxygen atoms. The coordination sphere is slightly offset by 4° from a perfectly linear P–Au–N geometry. The Au^I cation is shifted in the rough direction of the anion but the low degree of deformation is in the range of a packing effect and may be unaffected by the secondary interaction.

The observed unselective coordination is not surprising as a small but well-characterised number of Au^I pyridine complexes have been described.[88] Complexes **5**, **6** and **7** nevertheless demonstrate the selectivity for the softer phosphorus donor in a direct competition between the alternative coordination sites. The driving force for the formation of the homopolymer **11** over a cationic P–Au–P complex may be the low solubility of the former. While this demonstrates the limits in the selectivity of **4** it also emphasises that both coordination sites offer donors capable of forming strong dative bonds.

Heterobimetallic polymers, the target compounds of this study, could be obtained combining Zn^{II} and Hg^{II} halides. The emerging polymer structures all share the same overall formula $[ZnX_2(TRIP\text{-}Py)_2Hg_2X_4]^1_\infty$ (X = Cl (**12**), Br (**13**), I (**14**)) but differ substantially with respect to structural arrangement and porosity (Figure 14).

12 is a perfect combination of the structural motives presented in the previous sections and crystallises in the triclinic space group $P\bar{1}$ with $Z = 2$ (Figure 15). In contrast to the discrete Au-Zn complex this polymer displays a stretched geometry of the ligands around the Zn^{II} cation in a tetrahedral coordination sphere leading to thin polymer strands along [2 2 1]. A close

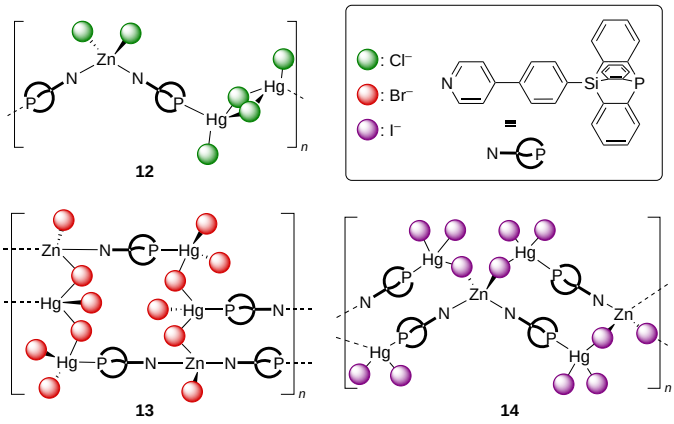

Fig. 14 Schematic representations of the Zn^{II}/Hg^{II} coordination polymers **12**-**14**.

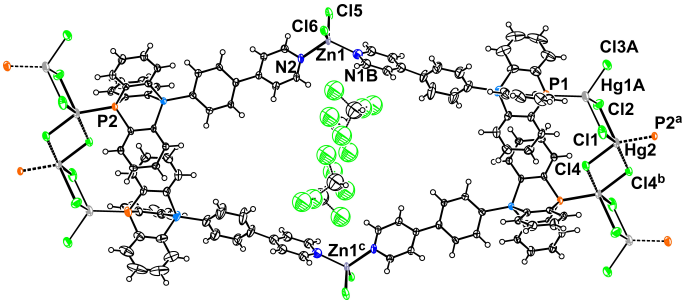

Fig. 15 Displacement ellipsoid plot of **12** (50% probability). The minority conformers of the main residue disorders have been omitted for clarity. Selected interatomic distances (Å): Zn1–N1B 2.029(7), Zn1–N2 2.079(5), Zn1–Cl5 2.2219(17), Zn1–Cl6 2.232(2), Hg1A–P1 2.403(3), Hg1A–Cl1 2.544(2), Hg1–Cl2 2.592(3), Hg1–Cl3A 2.442(5), Hg2–P2^a 2.3957(16), Hg2–Cl1 2.676(2), Hg2–Cl2 2.8576(19), Hg2–Cl4 2.3632(3), Hg2–Cl4^b 3.2193(18); Symmetry operations a: $2-x, 2-y, 1-z$; b: $-1-x, -1-y, -z$.

contact occurs between Hg2 and the chlorido ligand Cl4^b of a neighbouring chain with a distance of 3.2192(18) Å. If this interaction is perceived as topologically relevant, **12** represents a double stranded 1D polymer. The cavity between each $ZnCl_2$ pair in a double strand is occupied by one chloroform molecule disordered around a centre of inversion. These solvent-filled cavities are isolated, and no extended pores exist in the structure of **12**.

In contrast, **13** and **14** display more complex arrangements in which the halide ligands act as bridges between Zn^{II} and Hg^{II} cations. **13** crystallises in the triclinic space group $P\bar{1}$ with $Z = 2$ and features trinuclear $[ZnHg_2Br_6]$ arrangements (Figure 16). The Zn1 tetrahedron shares a corner with the Hg1 coordination sphere. The latter is the least regular as there are four Hg···Br contacts of different proximity.
P1^a, Br3 and Br4 subtend unexceptional ligand-cation distances and form a rather regular triangle about Hg1. Two significantly longer Hg···Br interactions complete the coordination sphere to a trigonal pyramid or a trigonal bipyramid: Hg1–Br2 amounts to 3.2648(17) Å, and the even longer Hg1···Br6 contact with

View Article Online
DOI: 10.1039/D2DT00728B

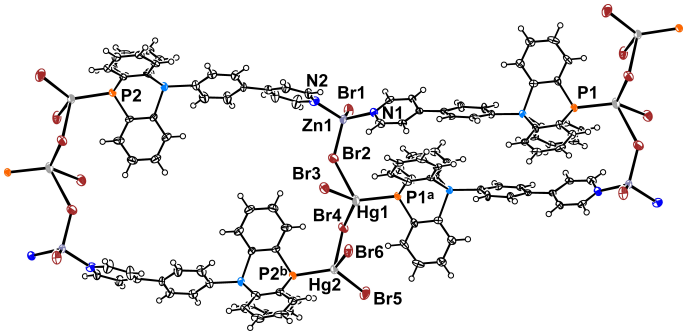

Fig. 16 Displacement ellipsoid plot of **13** (50% probability). Selected interatomic distances (Å): Zn1–N1 2.048(7), Zn1–N2 2.054(8), Zn1–Br1 2.3520(18), Zn1–Br2 2.3870(18), Hg1–Br2 3.2648(17), Hg1–Br3 2.4982(15), Hg1–Br4 2.6508(15), Hg1–P1^{a} 2.440(3), Hg1···Br6 3.4317(17), Hg2–Br4 2.9142(15), Hg2–Br5 2.5118(16), Hg2–Br6 2.6071(15), Hg1–P2^{b} 2.431(3); τ_4(Zn1) = 0.88, Var(X-Zn1-Y) = 41.9 °^{2}, τ_4(Hg1) = 0.80, Var(X-Hg1-Y) = 398.79 °^{2}, τ_4(Hg2) = 0.84, Var(X-Hg1-Y) = 158.9 °^{2}; Symmetry operations a: $-x, -y, 2-z$; b: $-x, 2-y, 1-z$.

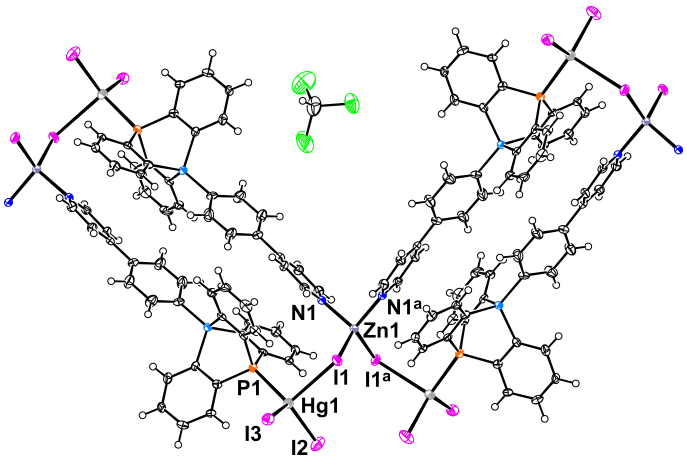

Fig. 17 Displacement ellipsoid plot of **14** (50% probability). Selected interatomic distances (Å): Zn1–N1 2.045(5), Zn1–I1 2.5655(11), Hg1–I1 3.0950(11), Hg1–I2 2.6702(10), Hg1–I3 2.7416(9), Hg1–P1 2.4909(17); τ_4(Zn1) = 0.94, Var(X-Zn1-Y) = 61.8 °^{2}, τ_4(Hg1) = 0.85, Var(X-Hg1-Y) = 100.5 °^{2}; Symmetry operation a: $1-x, y, 0.5-z$.

3.4317(17) Å roughly matches the sum of the van der Waals radii.[89,90] These more distant coordination partners Br2 and Br6 are engaged in shorter bonds to Zn1 and Hg2, respectively. The two TRIP-Py ligands attached to Zn1 adopt a stretched geometry like in **12**. The polymer propagates along [0 2 −1] and displays two structurally different repeat units. The first has the double stranded connection between two pairs of metal cations that share a corner of their coordination sphere while in the second repetition unit the double stranded connection occurs between pairs of more distant metal cations that do not share a corner. The latter does not lead to a cavity in the structure as it is relatively flat and occupied with triptycene phenylene rings of neighbouring polymer strands. Hence, **13** is not a solvate at all.

Compound **14** crystallises in the monoclinic space group $C2/c$ with $Z = 4$ (Figure 17). This polymer along c is single stranded as the connection point of each repetition unit is a single Zn^{II} cation. Both iodido ligands of Zn1 are shared corners with a Hg^{II} cation. The latter are equivalent by symmetry as Zn1 resides on the twofold rotation axis. Neighbouring strands are not related by noteworthy directional interactions. A tight channel along [1 0 1] with a limiting pore diameter of 4.26 Å is occupied by two chloroform molecules per asymmetric unit.

The selectivity of the ligand towards the combination of Zn^{II} and Hg^{II} naturally raises the question which site will be preferred by the intermediate Cd^{II} cation. The reaction of $CdBr_2$ with **4** gives the monometallic 2D coordination polymer $[Cd_2Br_4(TRIP\text{-}Py)_2(HOEt)]^2_\infty \cdot MeCN$ (**15**). It crystallises in the monoclinic space group $P2_1/c$ with $Z = 4$ with two symmetry independent Cd^{II} cations (Figure 18). Each Cd^{II} cation is coordinated by one terminal and one bridging bromido ligand. The latter form a one dimensional $[Cd\text{-}Br]_\infty$ chain along [0 0 1]. For Cd1 the octahedral coordination sphere is completed by two TRIP-Py pyridyl moieties and one ethanol molecule while the trigonal bipyramidal sphere around Cd2 is completed by two of the TRIP-Py P donors. This

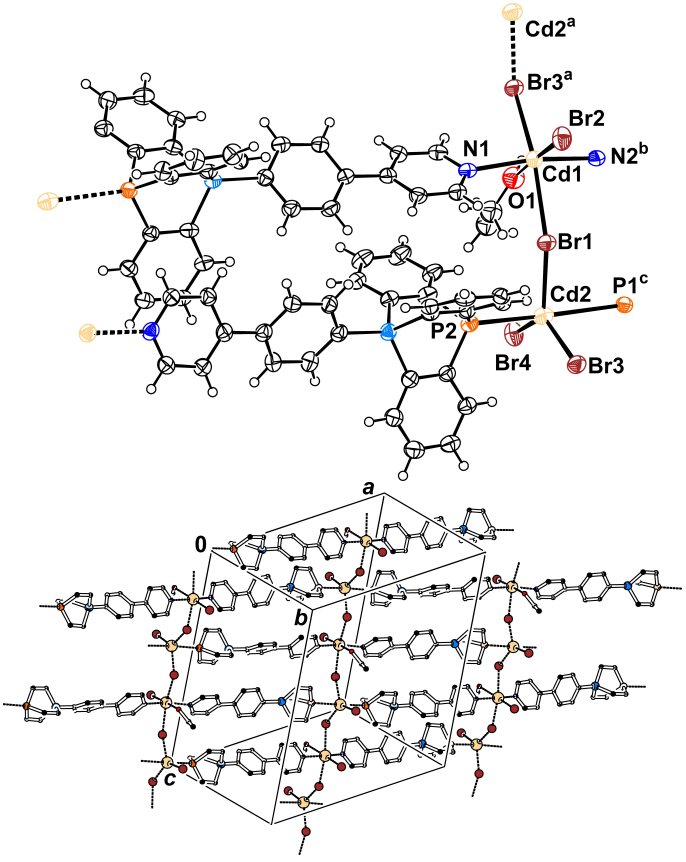

Fig. 18 (top) Displacement ellipsoid plot of **15** (50% probability). Selected interatomic distances (Å): Cd1–N1 2.315(4), Cd2–N2^{b} 2.306(4), Cd1–Br1 2.9029(17), Cd1–Br2 2.6030(16), Cd1–Br3^{a} 2.8074(17), Cd1–O1 2.608(5), Cd2–P1^{c} 2.949(2), Cd2–P2 2.873(2), Cd2–Br1 2.6258(16), Cd2–Br3 2.6302(16), Cd2–Br4 2.5475(16); Var(X-Cd1-Y) = 75.4 °^{2}, τ_5(Cd2) = 0.73 (8.4% along Berry Pseudorotation Coordinate); Symmetry operations a: $x, 0.5-y, z-0.5$; b: $x-1, 0.5-y, z-0.5$; c: $x-1, y, z$; d: $x, 0.5-y, z-0.5$. (bottom) Packing of **15**. Hydrogen atoms, solvent molecules have been omitted and the triptycene wings simplified for clarity.

View Article Online
DOI: 10.1039/D2DT00728B

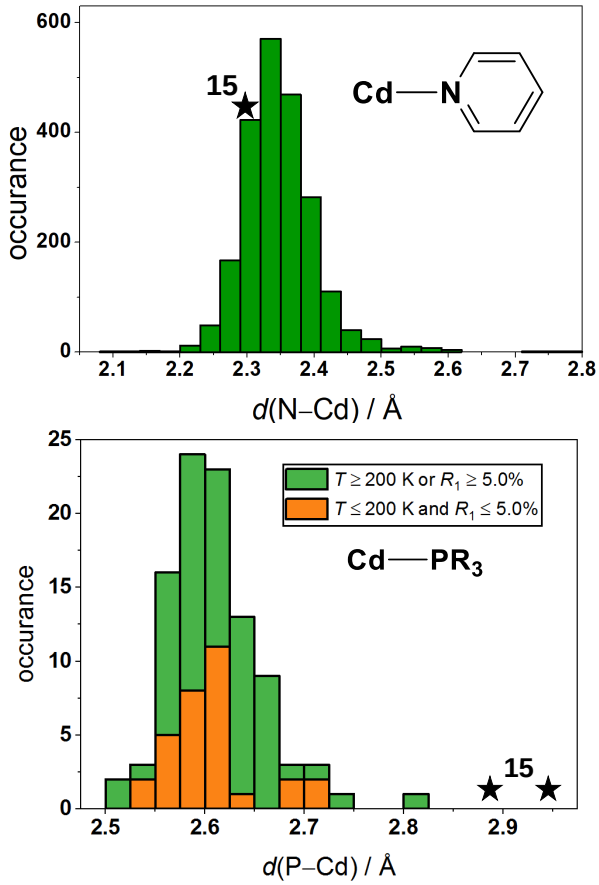

Fig. 19 Histograms of the N−Cd and P−Cd distances in Cd pyridyl complexes and Cd tertiary phosphine complexes respectively from the CSD and the values of compound **15**. For the N−Cd plot all structures with disorders, errors, $T \leq 200$ K or $R_1 \leq 0.05$ were excluded. For the P−Cd plot due to the low number of database entries only disordered structures and those with errors were excluded.

connects the $CdBr_2$ strands along [4 0 1] completing the two dimensional polymer in the *ac* plane.

The packing is rather tight with only one slim acetonitrile molecule in the small cavity between the polymer layers. While the Cd−N contacts are of regular length compared to structures retrieved from the database, the Cd−P contacts are remarkably long with interatomic distances both beyond 2.85 Å, longer than any other Cd−phosphine contact we could find in the CSD (Figure 19).[67] The directional nature of this contact clearly indicates a bonding interaction, and the broad window for interatomic distances is characteristic for d^{10} cations. This will surely be a result of the large steric demand of the triptycene scaffold and the occupation of the sterically more encumbered axial positions of the trigonal bipyramidal coordination sphere. The contrary is true for the bromido ligands around Cd2 which move much closer to Cd2 compared to the octahedral Cd1.

3 Conclusion

The compounds obtained with TRIP-Py clearly display its ability for selective coordination according to the HSAB principle. In the presence of two different cations, well-ordered bimetallic complexes are obtained. These target products may be discrete oligonuclear complexes when the Pearson soft moiety corresponds to AuCl or coordination polymers for Hg^{II} halides. The existence of monometallic polymers demonstrates that the selectivity can be compromised under certain conditions: the driving force in the formation of the Au^{I} polymer **11** is its insolubility. For the lighter coinage metal cation Ag^{I}, such a low solubility might even find an interesting application in antimicrobial activity.[91,92] The homometallic polymer **15** reflects the intermediate Pearson character of Cd^{II} but shows a clear preference towards the pyridyl donor as the Cd−P contacts are the longest ever reported. With respect to future work, polymer **15** represents a key compound, indicating how coordination networks extending in more dimensions and featuring higher porosity may become accessible. One can imagine to replace the bromido ligands by longer spacers such as terephthalates commonly used in MOF chemistry. Thus, TRIP-Py may act as a neutral and semi-rigid connector in MOF structures comparable to the role of 4,4'-bipyridine in MOF-508[93] but with the additional benefit of Pearson selectivity. Beyond the entirely structural aspects of TRIP-Py, the properties of the phosphatriptycene moiety have barely been investigated and offer a large playground for the development of potential applications.

Author Contributions

Conceptualization: H.G.; investigation: H.G., L.G., F.F.; supervision: U.E.; writing – original draft: H.G.; writing – review & editing: all authors. All authors have read and agreed to the published version of the manuscript.

Conflicts of interest

There are no conflicts to declare.

Acknowledgements

The authors acknowledge the German Academic Scholarship Foundation for a fellowship to Hans Gildenast. Furthermore we want to express our gratitude for the support from the One Hundred-Talent Program of Shanxi Province. Finally we would like to thank Dr. Carsten Paulmann for his help and support with the measurements at the DESY.

Notes and references

1 S. R. Batten, S. M. Neville and D. R. Turner, *Coordination Polymers*, Royal Society of Chemistry, Cambridge, 2008.
2 M. Tran, K. Kline, Y. Qin, Y. Shen, M. D. Green and S. Tongay, *Appl. Phys. Rev.*, 2019, **6**, 041311.
3 *Metal-Organic Frameworks*, ed. H. García and S. Navalón, Wiley-VCH Verlag GmbH & Co. KGaA, Weinheim, Germany, 2018.
4 A. D. Burrows, *Angew. Chem. Int. Ed.*, 2017, **56**, 1449.
5 A. Ejsmont, J. Andreo, A. Lanza, A. Galarda, L. Macreadie, S. Wuttke, S. Canossa, E. Ploetz and J. Goscianska, *Coord. Chem. Rev.*, 2021, **430**, 213655.
6 T. Gorai, W. Schmitt and T. Gunnlaugsson, *Dalton Trans.*, 2021, **50**, 770–784.

View Article Online
DOI: 10.1039/D2DT00728B

7 L. K. Cadman, M. F. Mahon and A. D. Burrows, *Dalton Trans.*, 2018, **47**, 2360–2367.
8 Q. Wang and D. Astruc, *Chem. Rev.*, 2020, **120**, 1438–1511.
9 L. Jiao, Y. Wang, H.-L. Jiang and Q. Xu, *Adv. Mater.*, 2017, 1703663.
10 M. Mutiah, S. Rochat, I. Amura, A. D. Burrows and E. A. Emanuelsson, *Chem. Eng. Process.*, 2021, **161**, 108315.
11 Y. Journaux, J. Ferrando-Soria, E. Pardo, R. Ruiz-Garcia, M. Julve, F. Lloret, J. Cano, Y. Li, L. Lisnard, P. Yu, H. Stumpf and C. L. M. Pereira, *Eur. J. Inorg. Chem.*, 2018, **2018**, 228–247.
12 M. Lippi and M. Cametti, *Coord. Chem. Rev.*, 2021, **430**, 213661.
13 Y. Song, R. Fan, J. Fan, K. Xing, X. Du, P. Wang and Y. Yang, *Dalton Trans.*, 2016, **45**, 16422–16432.
14 A. Ahmed, S. Seth, J. Purewal, A. G. Wong-Foy, M. Veenstra, A. J. Matzger and D. J. Siegel, *Nat. Commun.*, 2019, **10**, 1568.
15 S. Zhang, S. Zhang, S. Luo and D. Wu, *Coord. Chem. Rev.*, 2021, **445**, 214059.
16 D.-W. Lim and H. Kitagawa, *Chem. Rev.*, 2020, **120**, 8416–8467.
17 C.-H. Chuang and C.-W. Kung, *Electroanalysis*, 2020, **32**, 1885–1895.
18 W. W. Wei, L. P. Lu, S. S. Feng, M. L. Zhu and U. Englert, *Acta Crystallogr., Sect. B: Struct. Sci.*, 2021, **77**, 591–598.
19 S. Horike, N. Ma, Z. Fan, S. Kosasang and M. M. Smedskjaer, *Nano Lett.*, 2021, **21**, 6382–6390.
20 M. Kremer and U. Englert, *Z. Kristallogr. - Cryst. Mater.*, 2018, **233**, 437–452.
21 S. van Terwingen, N. Nachtigall, B. Ebel and U. Englert, *Cryst. Growth Des.*, 2021, **21**, 2962–2969.
22 D. Bansal, S. Pandey, G. Hundal and R. Gupta, *New J. Chem.*, 2015, **39**, 9772–9781.
23 F. A. A. Paz, J. Klinowski, S. M. F. Vilela, J. P. C. Tomé, J. A. S. Cavaleiro and J. Rocha, *Chem. Soc. Rev.*, 2012, **41**, 1088–1110.
24 M. Du, C.-P. Li, C.-S. Liu and S.-M. Fang, *Coord. Chem. Rev.*, 2013, **257**, 1282–1305.
25 E. C. Constable and C. E. Housecroft, *Comprehensive Inorganic Chemistry II*, Elsevier, 2013, vol. 290, pp. 1–29.
26 C. Hu and U. Englert, *Angew. Chem., Int. Ed. Engl.*, 2005, **44**, 2281–2283.
27 R. G. Pearson, *J. Am. Chem. Soc.*, 1963, **85**, 3533–3539.
28 M. Kondracka and U. Englert, *Inorg. Chem.*, 2008, **47**, 10246–10257.
29 Q. Guo, C. Merkens, R. Si and U. Englert, *CrystEngComm*, 2015, **17**, 4383–4393.
30 B. Chen, F. R. Fronczek and A. W. Maverick, *Inorg. Chem.*, 2004, **43**, 8209–8211.
31 L. Carlucci, G. Ciani, D. M. Proserpio and M. Visconti, *CrystEngComm*, 2011, **13**, 5891.
32 Y. Zhang, B. Chen, F. R. Fronczek and A. W. Maverick, *Inorg. Chem.*, 2008, **47**, 4433–4435.
33 A. D. Burrows, K. Cassar, M. F. Mahon and J. E. Warren, *Dalton Trans.*, 2007, 2499–2509.
34 V. D. Vreshch, A. B. Lysenko, A. N. Chernega, J. A. K. Howard, H. Krautscheid, J. Sieler and K. V. Domasevitch, *Dalton Trans.*, 2004, 2899–2903.
35 V. D. Vreshch, A. B. Lysenko, A. N. Chernega, J. Sieler and K. V. Domasevitch, *Polyhedron*, 2005, **24**, 917–926.
36 A. D. Burrows, C. G. Frost, M. F. Mahon, P. R. Raithby, C. L. Renouf, C. Richardson and A. J. Stevenson, *Chem. Commun.*, 2010, **46**, 5067–5069.
37 Y. Zhang and A. W. Maverick, *Inorg. Chem.*, 2009, **48**, 10512–10518.
38 Y. Han, H. Zheng, K. Liu, H. Wang, H. Huang, L.-H. Xie, L. Wang and J.-R. Li, *ACS Appl. Mater. Interfaces*, 2016, **8**, 23331–23337.
39 H. Gildenast, S. Nölke and U. Englert, *CrystEngComm*, 2020, **22**, 1041–1049.
40 H. Gildenast, F. Busse and U. Englert, *Cryst. Growth Des.*, 2021, **21**, 5807–5817.
41 P. Steinhoff, R. Steinbock, A. Friedrich, B. G. Schieweck, C. Cremer, K.-N. Truong and M. E. Tauchert, *Dalton Trans.*, 2018, **47**, 10439–10442.
42 J. Takaya, M. Hoshino, K. Ueki, N. Saito and N. Iwasawa, *Dalton Trans.*, 2019, **48**, 14606–14610.
43 Y. Cabon, I. Reboule, M. Lutz, R. J. M. Klein Gebbink and B.-J. Deelman, *Organometallics*, 2010, **29**, 5904–5911.
44 J. P. Schroers, M. N. Kliemann, J. M. A. Kollath and M. E. Tauchert, *Organometallics*, 2021, **40**, 3893–3906.
45 X. Tan, X. Chen, J. Zhang and C.-Y. Su, *Dalton Trans.*, 2012, **41**, 3616–3619.
46 F. Hung-Low, K. K. Klausmeyer and J. B. Gary, *Inorg. Chim. Acta*, 2009, **362**, 426–436.
47 A. Renz, M. Penney, R. Feazell and K. K. Klausmeyer, *J. Chem. Crystallogr.*, 2012, **42**, 1129–1137.
48 K. K. Klausmeyer, R. P. Feazell and J. H. Reibenspies, *Inorg. Chem.*, 2004, **43**, 1130–1136.
49 X. Tan, L. Li, J. Zhang, X. Han, L. Jiang, F. Li and C.-Y. Su, *Chem. Mater.*, 2012, **24**, 480–485.
50 C.-Q. Zhao, M. C. Jennings and R. J. Puddephatt, *J. Inorg. Organomet. Polym Mater.*, 2008, **18**, 143–148.
51 J. Kühnert, I. Císarová, M. Lamac and P. Stepnicka, *Dalton Trans.*, 2008, 2454–2464.
52 N.-Y. Li, Z.-G. Ren, D. Liu, R.-X. Yuan, L.-P. Wei, L. Zhang, H.-X. Li and J.-P. Lang, *Dalton Trans.*, 2010, **39**, 4213–4222.
53 T. Zhang, K. Wang, C. Ji and X. Meng, *J. Inorg. Organomet. Polym Mater.*, 2014, **24**, 865–873.
54 J.-F. Wang, S.-Y. Liu, C.-Y. Liu, Z.-G. Ren and J.-P. Lang, *Dalton Trans.*, 2016, **45**, 9294–9306.
55 T. Zhang, C. Chen, Y. Qin and X. Meng, *Inorg. Chem. Commun.*, 2006, **9**, 72–74.
56 X. Wang, J. Huang, S. Xiang, Y. Liu, J. Zhang, A. Eichhöfer, D. Fenske, S. Bai and C.-Y. Su, *Chem. Commun.*, 2011, **47**, 3849–3851.
57 U. Siemeling, T. Klemann, C. Bruhn, J. Schulz and P. Štěp-

View Article Online
DOI: 10.1039/D2DT00728B

ička, *Dalton Trans.*, 2011, **40**, 4722–4740.
58 X. Wang, J. Feng, J. Huang, J. Zhang, M. Pan and C.-Y. Su, *CrystEngComm*, 2010, **12**, 725–729.
59 M. K. Penney, R. Giang, M. A. Burroughs and K. K. Klausmeyer, *Polyhedron*, 2015, **87**, 43–54.
60 S. Welsch, C. Lescop, R. Réau and M. Scheer, *Dalton Trans.*, 2009, 2683–2686.
61 A. Y. Baranov, M. I. Rakhmanova, D. G. Samsonenko, S. F. Malysheva, N. A. Belogorlova, I. Y. Bagryanskaya, V. P. Fedin and A. V. Artem'ev, *Inorg. Chim. Acta*, 2019, **494**, 78–83.
62 Y. Liu, S. Lv, D. Liu and F. Song, *Acta Biomater.*, 2020, **116**, 16–31.
63 Z.-W. Ruan, X. Zhang, A.-Y. Pang, F.-R. Dai and Z.-N. Chen, *Inorg. Chem. Commun.*, 2020, **116**, 107916.
64 A. V. Artem'ev, A. Y. Baranov, M. I. Rakhmanova, S. F. Malysheva and D. G. Samsonenko, *New J. Chem.*, 2020, **44**, 6916–6922.
65 A. J. Ashe, *J. Am. Chem. Soc.*, 1971, **93**, 3293–3295.
66 H. Shet, U. Parmar, S. Bhilare and A. R. Kapdi, *Org. Chem. Front.*, 2021, **8**, 1599–1656.
67 C. R. Groom, I. J. Bruno, M. P. Lightfoot and S. C. Ward, *Acta Crystallogr., Sect. B: Struct. Sci.*, 2016, **72**, 171–179.
68 T. Agou, J. Kobayashi and T. Kawashima, *Chem. Lett.*, 2004, **33**, 1028–1029.
69 F. J. M. Freijee and C. H. Stam, *Acta Crystallogr., Sect. B: Struct. Crystallogr. Cryst. Chem.*, 1980, **36**, 1247–1249.
70 C. Jongsma, J. P. de Kleijn and F. Bickelhaupt, *Tetrahedron*, 1974, **30**, 3465–3469.
71 M. W. Drover, K. Nagata and J. C. Peters, *Chem. Commun.*, 2018, **54**, 7916–7919.
72 L. Hu, D. Mahaut, N. Tumanov, J. Wouters, R. Robiette and G. Berionni, *J. Org. Chem.*, 2019, **84**, 11268–11274.
73 Y. Cao, J. W. Napoline, J. Bacsa, P. Pollet, J. D. Soper and J. P. Sadighi, *Organometallics*, 2019, **38**, 1868–1871.
74 S. Kawamorita, T. Miyazaki, H. Ohmiya, T. Iwai and M. Sawamura, *J. Am. Chem. Soc.*, 2011, **133**, 19310–19313.
75 L. Hu, D. Mahaut, N. Tumanov, J. Wouters, L. Collard, R. Robiette and G. Berionni, *Dalton Trans.*, 2021, **50**, 4772–4777.
76 S. Konishi, T. Iwai and M. Sawamura, *Organometallics*, 2018, **37**, 1876–1883.
77 T. Iwai, S. Konishi, T. Miyazaki, S. Kawamorita, N. Yokokawa, H. Ohmiya and M. Sawamura, *ACS Catal.*, 2015, **5**, 7254–7264.
78 H. Tsuji, T. Inoue, Y. Kaneta, S. Sase, A. Kawachi and K. Tamao, *Organometallics*, 2006, **25**, 6142–6148.
79 D. Hellwinkel and W. Schenk, *Angew. Chem., Int. Ed. Engl.*, 1969, **8**, 987–988.
80 C. Eaborn, *J. Chem. Soc.*, 1952, 2840.
81 R. Damrauer, R. A. Simon and B. Kanner, *Organometallics*, 1988, **7**, 1161–1164.
82 N. L. Allinger, *Journal of the American Chemical Society*, 1977, **99**, 8127–8134.
83 PerkinElmer, *Chem3D*, 2020.
84 Y. Mo and J. Gao, *Accounts of chemical research*, 2007, **40**, 113–119.
85 H. Ube, Y. Yasuda, H. Sato and M. Shionoya, *Nature Communications*, 2017, **8**, 14296.
86 A. W. Addison, T. N. Rao, J. Reedijk, J. van Rijn and G. C. Verschoor, *J. Chem. Soc., Dalton Trans.*, 1984, 1349–1356.
87 C. F. Macrae, P. R. Edgington, P. McCabe, E. Pidcock, G. P. Shields, R. Taylor, M. Towler and J. van de Streek, *J. Appl. Crystallogr.*, 2006, **39**, 453–457.
88 Y. Inoguchi, B. Milewski-Mahrla and H. Schmidbaur, *Chemische Berichte*, 1982, **115**, 3085–3095.
89 A. Bondi, *J. Phys. Chem.*, 1964, **68**, 441–451.
90 S. S. Batsanov, *Russian Chemical Bulletin*, 1995, **44**, 18–23.
91 P. Smoleński, S. W. Jaros, C. Pettinari, G. Lupidi, L. Quassinti, M. Bramucci, L. A. Vitali, D. Petrelli, A. Kochel and A. M. Kirillov, *Dalton transactions (Cambridge, England : 2003)*, 2013, **42**, 6572–6581.
92 S. W. Jaros, A. Krogul-Sobczak, B. Bażanów, M. Florek, D. Poradowski, D. S. Nesterov, U. Śliwińska-Hill, A. M. Kirillov and P. Smoleński, *Inorganic Chemistry*, 2021, **60**, 15435–15444.
93 B. Chen, C. Liang, J. Yang, D. S. Contreras, Y. L. Clancy, E. B. Lobkovsky, O. M. Yaghi and S. Dai, *Angewandte Chemie (International ed. in English)*, 2006, **45**, 1390–1393.